JOURNAL OF MATERIALS SCIENCE **39** (2004) 6705–6721

The wear behaviour of oxide ceramics-A Review

W. M. RAINFORTH
Department of Engineering Materials, The University of Sheffield, Mappin Street, Sheffield S1 3JD, UK
E-mail: m.rainforth@shef.ac.uk

The paper reviews the wear behaviour of oxide ceramics. Wear maps are considered and consequently mild and severe wear are defined. Since the use of ceramics in engineering applications require operation in the mild wear regime, the paper concentrates on mild wear mechanisms, but also considers factors which control the transition to severe wear. Within the mild wear regime, the formation of tribofilms are discussed and the manner in which dislocation activity leads to the wear transition is considered. The wear of so-called ceramic nanocomposites, for which no time dependent wear transition has yet been observed, is considered and the reasons for enhanced performance discussed. The role of transformation toughening in zirconia ceramics is considered in detail, and reasons for the generally poor wear response of these materials defined.

1. Introduction

For structural ceramics, the only manufacturing sector that has seen major growth is in tribological applications. This has largely been because of the pressure to produce components with longer life times and/or reduced servicing down time. In many cases, the only realistic option in achieving greater performance from a metal tribo-element has been to replace it by a ceramic component, where the high hardness (typically >16 GPa), potentially low friction and excellent corrosion resistance are three of the most important material attributes. While the low fracture toughness of ceramics has hindered much of their use in structural applications where a tensile stress is dominant, it has been found that low fracture toughness is less of a problem in tribological applications. Ceramics have proved reliable in a range of demanding applications, such as mechanical seals (Al_2O_3, Si_3N_4, SiC), prosthetic devices (Al_2O_3, Al_2O_3-ZrO_2) and ball bearings (Si_3N_4), among many examples. Nevertheless, fracture toughness does remain a major concern to design engineers and consequently the uptake of these materials has been slower than it might otherwise have been.

The gradual increase in the use of ceramics in engineering components has somewhat lagged behind the substantial academic interest in the tribological properties of these materials, with a large data base of mechanistic understanding ensuing [1–90]. The wear of ceramics has been broadly separated into 'mild' and 'severe' [1, 3], which, unlike the metal equivalent, are well defined, see Section 3. The evidence to date suggests that a ceramic will be useful as a commercial tribological component provided the specific wear rate is $<10^{-6}$ mm^3/Nm, which is the upper limit for mild wear [1, 3].

The understanding of the material removal mechanisms in the mild regime has not received sufficient attention, despite being the most important, and consequently is the least understood area. The majority of wear studies report the worn surface structures and specific wear rates that place them firmly in the severe wear regime and are therefore of little use in commercial applications. The mild wear regime leads, by definition, to smoothing of the worn surface. It remains far from clear exactly how material is lost as wear debris in such a way that the asperity height is reduced.

The formation of surface layers (also referred to as tribo-layers, transfer layers, compacted layers and many other descriptions) is a common observation and such layers are known to modify both friction and wear behaviour (see [2] and references therein). However, the origins of such layers may be quite different, depending on whether they arose from compaction of wear debris or from reaction of the substrate with the environment. In all cases, the structure is very different to that of the substrate, and consequently it is not surprising that they strongly influence wear. However, there remains much work to do on the understanding of the properties of such films and consequently how they can be modified to minimise friction and wear. This review will consider the current knowledge with respect to surface films in the mild wear regime, in particular those formed through reaction with the substrate, that appear to be a fundamental aspect of mild wear. However, the nature of layers that result from compaction of wear debris in the severe wear regime will not be considered for the reasons given above.

Most ceramics exhibit a wear transition from mild to severe wear, at some critical load (although this load depends on material, time of operation, sliding

speed and environment) [13, 26–28]. The transition is characterised by an increase in wear, often several orders of magnitude, and is associated with the onset of brittle fracture at the surface [6, 7, 12, 13, 25–27]. The specific wear rate in the severe regime is typically $>10^{-4}$ mm^3/Nm, which is therefore easily separated from the mild wear regime (although values closer to 10^{-6} mm^3/Nm can also be observed, in which case the term severe wear refers specifically to the surface roughening associated with fracture; the reasons for this are discussed later). Since any engineering component operating in the severe wear regime will have failed, the severe regime will not be considered in this review. However, the mechanisms leading up to the transition, particularly the time dependant aspects are especially important and will therefore be considered in some detail.

A parallel issue to the formation of surface films is the modification of the properties of the ceramic at its surface (e.g., hardness) by the environment. Free surface issues have not received much attention, even though the presence of water can substantially alter the hardness and crystallography of dislocation slip at the ceramic surface [13, 16, 17, 33, 35, 36]. This review will therefore critically examine the limited data in this area.

The low toughness of ceramics has remained a stumbling block for their wider use, although not as much in tribological applications as structural applications. Moreover, the wear transition from mild to severe wear is also obviously related to toughness (albeit in a complex manner), since the transition is associated with surface fracture. There have been a number of strategies used to improve the reliability of ceramics, falling into three broad categories: (a) the general reduction in microstructural scale, particularly grain size, and improved density, in an attempt to reduce the flaw size within the material; (b) the formation of duplex structures where one phase has nano-scopic dimensions and there is a carefully engineered thermal expansivity mismatch between the phases; (c) transformation toughening. Each area has seen some success. For example, Al_2O_3 hip joint prosthetics are now substantially more successful than they used to be as a result of a change in process conditions that has yielded a ceramic with increased density (by HIPing), and a smaller, more uniform grain size. Similarly, so-called Al_2O_3-SiC nanocomposites have been shown to have much greater resistance to surface fracture, and apparently the time dependent wear transition found in monolithic Al_2O_3 is removed in the nanocomposite. Finally, zirconia based ceramics offer the highest toughness of any ceramic, but have found very limited success in tribological applications. All three of these categories will be examined in this review.

It is not possible to cover all aspects of the wear of ceramics or all ceramic materials in one article. Consequently, the review will focus on the mild wear regime and will discuss only oxide based ceramics. While all wear mechanisms will be discussed, the discussion of erosion and, as noted above, severe wear will be limited.

2. Experimental procedure

2.1. Materials

High purity alumina (99.9%) was supplied by Dynamic Ceramic Ltd. in the form of machined wear pins. The 3 mol% TZP material was manufactured using commercial Dai-ichi^{TM} powders, also supplied in finished form by Dynamic Ceramic Ltd., Crewe Hall, Crewe, (UK). The final shape of the wear pins (10 mm diameter round with 30° truncated cone giving a 3 mm diameter contact face) was obtained by diamond grinding, and the contacting surface was diamond lapped to a high surface finish. The fracture toughness of this material was 8.1 MPa m (measured by indentation, at a load of 30 kg) and the hardness was 11.3 GPa.

Nanocomposites containing 2.5, 5, 10, 15 vol% SiC were manufactured from Alcan Chemicals Ltd. (UK) 99.5% Al_2O_3 and Ibiden Co. (Japan) β-SiC. The powders were dispersed in distilled water containing 0.2 wt% Dispex A40 dispersant (Allied Colloids) and ball milled using high purity alumina balls for 24 h. The slip was cast into a mould, dried and sintered at 1200°C for 2 h in argon. Discs were hot pressed in a graphite die at 1600°C for 2 h at a pressure of 25 MPa followed by annealing at 1300°C for 2 h in argon. This yielded monolithic ceramics with a density >99.5% theoretical and composites with >97% theoretical. An additional monolithic alumina sample was fabricated under identical conditions but only hot pressed for 1 h (i.e., hot pressed 1 h at 1600°C, 25 MPa, followed by annealing at 1300°C for 2 h in argon), to yield a ceramic with a similar grain size to that of the composites. The density of this monolith was, within experimental error, the same as the monolith hot pressed for 2 h at 1600°C.

2.2. Wear testing

Wear testing was undertaken on several different machines, depending on the quantity of material available. The most reproducible results were obtained from a tri-pin-on-disc machine, the full details of which are given elsewhere [62]. Great care is required in ceramic wear experiments to ensure that the pins are flat and that each protrudes from the head to no more than 5 μm of each other. Despite these precautions, the initial apparent contact area is unavoidably relatively small and therefore the true contact stress would have been higher than expected from the applied load and specimen geometry. Tests were undertaken under dry sliding and distilled water lubrication. Loads were varied in the range 6–50 N/pin. In most cases, a sliding speed of 0.24 m/s was used (other speeds are indicated in the text). Wear rates were measured by weight loss of the pin, with measurements made to an accuracy of $\pm 2 \times 10^{-5}$ g. An identical virgin wear pin was placed in the same medium as the test (i.e., the laboratory air, or distilled water etc.) for the same time as the wear test and then weighed with the other pins. This allowed us to account for any changes to the weight of the pin as a result of fluid adsorption from the environment.

A variety of counterface materials were used, including a zirconia toughened alumina disc (supplied by Dynamic Ceramic, Crewe Hall, Crewe (UK)), an

8.5 mol% magnesia partially stabilised zirconia (Mg-PSZ), supplied by Coors Ceramics Ltd., Southfield, Scotland, (UK). The counterface discs were 90 mm diameter in diameter and 10 mm thick.

Both wear test materials were prepared by diamond lapping. The last stages of lapping were undertaken on a 0.1 μm diamond tin lap which provided a surface finish in the range 5–8 nm R_a, depending on material type. Back-thinned transmission electron microscopy (TEM) was used to verify that this preparation treatment removed the majority of damage associated with prior grinding and lapping.

2.3. Characterisation

Scanning electron microscopy (various microscopes) was used to examine worn surfaces and to determine the grain size (which was determined from thermally etched surfaces, using a Schwartz-Saltykoff analysis with in excess of 100 grains in each case).

Atomic force microscopy (AFM) was performed using a Digital Instruments (DI) Dimension 3000 Scanning Probe Microscope (SPM) operating in the contact mode. Standard silicon cantilevers with a pyramidal silicon tip was used to acquire images.

Samples for transmission electron microscopy (TEM) were produced by both back-thinning of the wear surface and in cross-section. In all cases, the samples were only taken when the wear rate was well into steady state and the wear volume was sufficient to have completely removed the original lapped surface. For cross-sectional samples, the position of the worn surface was first labelled with a sputter deposited gold coating (preferential erosion of the surface during ion milling can occur, and therefore it is important to know the location of the original surface with certainty). The sample preparation for both back thinning and longitudinal cross-section is detailed elsewhere [4, 13, 62, 66]. For the latter, following examination of each TEM specimen, further ion milling was undertaken to reveal new areas of the worn surface. In this way, approximately 1mm of worn surface was investigated for each TEM specimen. TEM was undertaken on a range of microscopes, although the majority of the work was undertaken on a Jeol 200CX microscope operating at 200 kV.

X-ray diffraction (XRD) (Philips model PW1710 diffractometer) was used to determine phase constitution of the test materials. For the 3Y-TZP materials, XRD confirmed that the test surface contained no detectable monoclinic zirconia after the lapping procedure.

3. Wear maps

Wear maps have been proposed by a number of researchers [1, 3, 5–11]. Adachi *et al.* [3] separate the maps into two types. The first class are defined as those that use the experimental variables as the axes, the most obvious examples being normal load and sliding velocity, but can also include temperature, sliding distance and so on. Such maps are generally straight forward to interpret. However, the disadvantage of such maps is that the wear rate is system specific, such that the wear rate read off a map for, e.g., a specific load, is unlikely to be transferable to another wear geometry/engineering system and therefore cannot be used for design.

The second type of map uses dimensionless axes. These tend to be more widely applicable and can cover a wide range of operating conditions [1, 3]. The most widely cited paper related to this is the work of Lim and Ashby [9], who used axes of normalised pressure and normalised velocity. Kong and Ashby [10] produced one such map for alumina, which showed a total of seven wear modes. There have been a number of variations on this theme, with a range of different dimensionless parameters suggested for the axes. Much work has been done since Lim and Ashby to extend wear maps and model behaviour therein, with the work of Adachi and Kato [1, 3] and Hsu and co-workers [6–8, 26–28] of particular note. Adachi *et al.* [1, 3] examined the wear of Al_2O_3, ZrO_2 and SiC in a pin on disc configuration. Test conditions provided a substantial range of specific wear rate, from 10^{-9} to 10^{-2} mm^3/Nm (smaller and larger than found for metallic wear), and a wide range of friction coefficient, from 0.1 to 1.1. Adachi *et al.* [3] proposed a new set of dimensionless parameters for a wear map. The severity of contact, $S_{c,m}$ is derived, based on Hertzian contact pressure, considering the maximum tensile stress, and using basic linear elastic fracture mechanics, to incorporate the relationship between critical flaw size and K_{1C}:

$$S_{c,m} = \frac{(1 + 10\,\mu)P_{max}\sqrt{d}}{K_{1C}}$$

where μ the friction coefficient, P_{max} is the maximum Hertzian contact pressure, d is the pre-existing crack length, and K_{1C} is the fracture toughness of the material. Mild wear exists for the condition:

$$S_{c,m} \leq C_m$$

where C_m is a constant.

Adachi *et al.* further define the thermal conditions required to give mild wear, taking account of the flash temperature rise from frictional heating and the consequent thermal shock effect on the ceramic. The critical condition for mild wear is defined as:

$$S_{c,t} \leq C_t$$

where C_t is a constant (i.e., the threshold value for mild wear) and $S_{c,t}$ is given by:

$$S_{c,t} = \frac{\gamma\mu}{\Delta T_s}\sqrt{\frac{\upsilon W HV}{k\rho c}}$$

where γ is the heat partition ratio, ΔT_s is the thermal shock resistance, k is the thermal conductivity, ρ the density, c is the specific heat υ is the sliding velocity and HV is the Vickers hardness. The thermal shock

resistance can be derived from:

$$\Delta T_s \propto \frac{(1-\upsilon)K_{1C}}{E\alpha\sqrt{\pi d}}$$

where α is the thermal expansion coefficient.

The experimentally determined limiting values for mild wear were reported as:

$$S_{c,m} \leq 6$$
$$S_{c,t} \leq 0.04$$

Adachi *et al.* [3] further developed the model to allow $S_{c,m}$ and $S_{c,t}$ to be determined without prior knowledge of μ, which clearly cannot be predicted, but must be determined experimentally.

Adachi *et al.* showed a linear relationship (albeit with considerable scatter) between $S_{c,m}$ and specific wear rate, with severe and mild wear falling on the same line, with similar levels of scatter, Fig. 1.

Using this definition of mild and severe wear, Kato and Adachi [1], investigated the dry and lubricated wear of Al_2O_3, ZrO_2 and SiC. Plotting the regimes of mild and severe wear on conventional load vs. sliding velocity maps indicated major differences between the size of the mild wear regime for the three materials, Fig. 2. The largest region for mild wear existed for SiC, while the smallest was for ZrO_2. Indeed, a sliding velocity of less than ~0.03 m/s is required to ensure mild wear

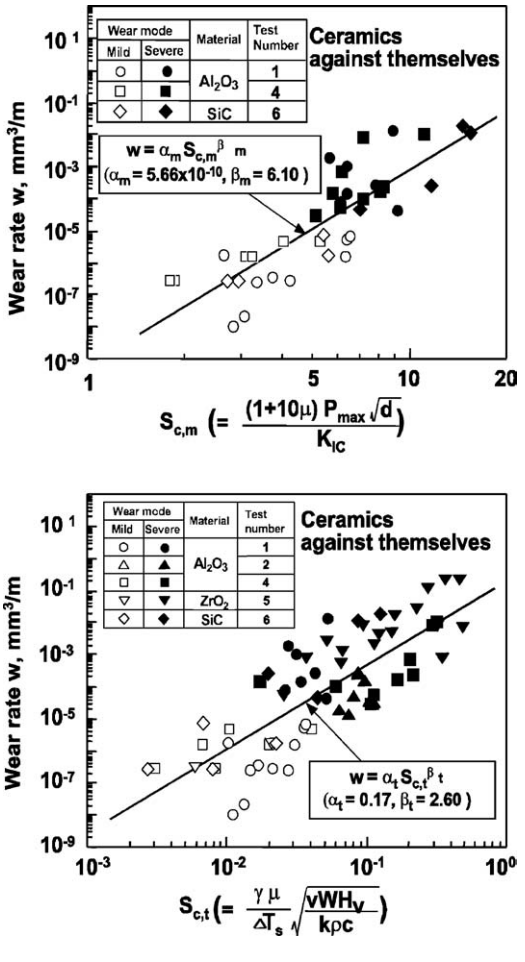

Figure 1 Wear rate against $S_{c,m}$ and $S_{c,t}$ (see text for definitions) for alumina, zirconia and silicon carbide. After Adachi and Kato [3].

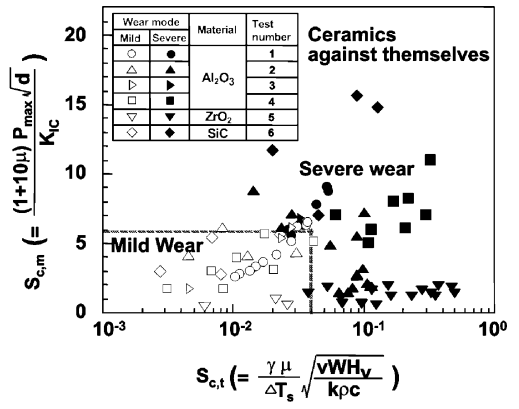

Figure 2 $S_{c,m}$ against $S_{c,t}$ (see text for definitions) for alumina, zirconia and silicon carbide. After Adachi and Kato [3].

for ZrO_2. This is related to its low thermal conductivity and is described in detail later. Interestingly, water lubrication greatly increased the extent of mild wear for Al_2O_3, but not for ZrO_2. Again, this will be discussed in detail later. The trends shown by Adachi and Kato are similar to those found by Hsu and co-workers, who have developed an alternative, but similar approach to wear mapping.

4. Mild wear in alumina and the wear transition

The mechanisms of material removal in the mild wear regime, as defined above by Adachi and Kato, are still poorly understood. The surfaces become, by definition, smoother than the starting state. As such, a clear understanding of this regime could lead to reduced wear rates and also improved methods of polishing ceramics, a point noted by Fischer and co-workers [32], for example. Although the surface may become smoother, some fine scale features are often present, for example, microscale abrasion, and differential wear between grains. However, it is clear that significant fracture is absent in this regime. Moreover, as described below, while dislocation activity may occur, it is usually constrained to below abrasive grooves, and does not appear to have any rate-limiting role in the mild wear rate. The question, therefore, is what is the rate limiting material removal mechanism? The following paragraphs review the evidence.

Fig. 3a gives an SEM image of the worn surface of a zirconia toughened alumina, clearly operating in the mild wear regime. There are two kinds of wear debris present, the smeared debris present as a band across the middle of the micrograph (the edge of the wear track) and the finer 'rolls' present as randomly distributed particles in the upper half of the micrograph (within the wear track). The main wear debris is similar in appearance to that observed on an explanted Al_2O_3 hip joint [25], as shown in Fig. 3b, also located at the edge of the contact region. Such films are known to be amorphous in many cases, and for the wear of Al_2O_3, have been shown to be aluminium hydroxide, or similar [e.g., 30].

The second type of wear debris in Fig. 3a are the rolls observed in the upper region. These rolls have been observed by many authors [e.g., 32, 37, 38], for a wide

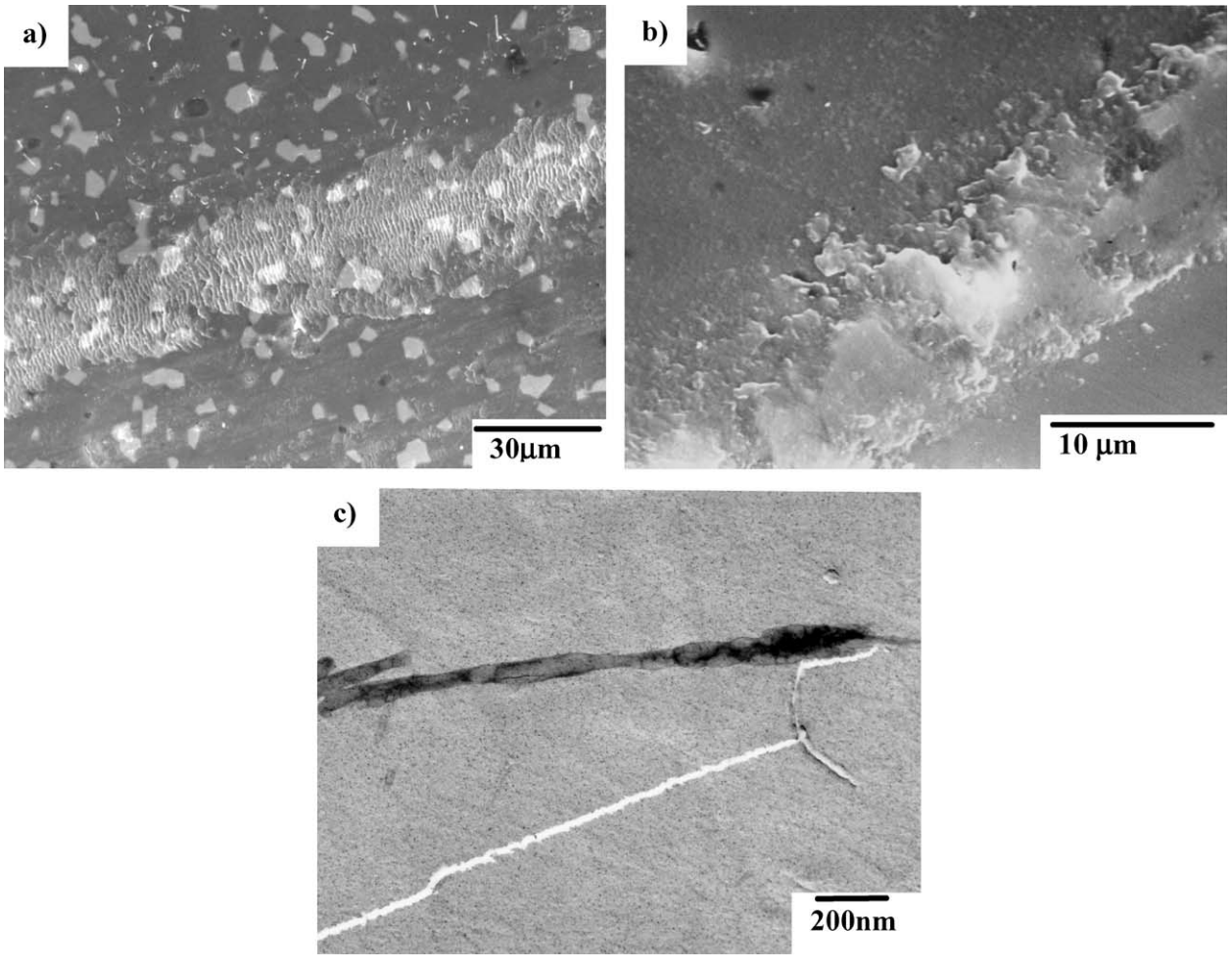

Figure 3 (a) SEM micrograph of the worn surface of a zirconia toughened alumina (worn against a 3Y-TZP at 0.016 m/s). Note the accumulated wear debris across the centre of the micrograph and the 'rolls' in the upper region of the wear track. (b) SEM micrograph of the edge of the wear track on an explanted alumina femoral head, which had been coupled with an alumina acetabular cup, operating in the mild wear regime. (c) TEM micrograph of a 'roll' supported on a carbon film, following removal from the worn surface in (a).

range of ceramics, including oxide and non-oxide. They are often believed to be beneficial to wear (since they coincide with low wear rates), even with suggestions being put forward that they could act as a 'low friction bearing' between the two surfaces. An acetate replica technique was used to remove these particles for subsequent examination in the TEM, the result of which is shown in Fig. 3c. The roll is amorphous and, apart from the shape, appears to be similar in most respects to the thin amorphous films observed on the surfaces of ceramics, such as that in Fig. 3a. Careful examination of the TEM micrograph in Fig. 3c suggests that the 'rolls' are made up of a rolled up sheet, rather than being a solid entity. This, and other evidence, suggests that the rolls are simply a result of removal of the amorphous tribo-film, which then roll-up because of the residual stress within the film (since the film is initially bonded to the substrate, but is a transformation product from the substrate, it will inevitably be under stress because of the different physical substructure size).

Fig. 4a gives a Nomarski contrast optical micrograph from an Al_2O_3 sample operating in the mild wear regime. Note the differential wear between grains (that will be considered later). Fig. 4b is a bright field TEM image from one of the grains that has worn the most (as shown by the reduced thickness in this region). There was no evidence of mechanical damage (i.e., no dislocation activity and no microfracture). However, the image shows a region where the thin surface tribolayer has been partially lost. This was the only evidence of material loss found in this grain and numerous other examples examined. This and other evidence suggests that the rate limiting material removal step is either the growth or detachment of such films. However, the evidence remains sparse and further investigations are required. Moreover, it would be interesting to know whether it is the growth or detachment of the film that is rate limiting, and what factors (e.g., material composition) that are important.

The formation of these thin tribofilms is quite distinct from the surface compacted layers, widely reported in the literature [e.g., 2]. The films described in the preceding paragraphs are difficult to observe, and require the use of careful microscopy or spectroscopy to detect them. In contrast, while compacted layers of wear debris often reduce wear rate and friction coefficient, they are a feature of relatively high wear rates, where there is large amounts of wear debris produced by fracture that are subsequently broken up by attrition. Consequently, these layers are usually (but not always) crystalline, and often nanocrystalline, which is almost certainly the origin of the wear reduction properties.

Most ceramics, including alumina, exhibit a load dependent wear transition, which is associated with a

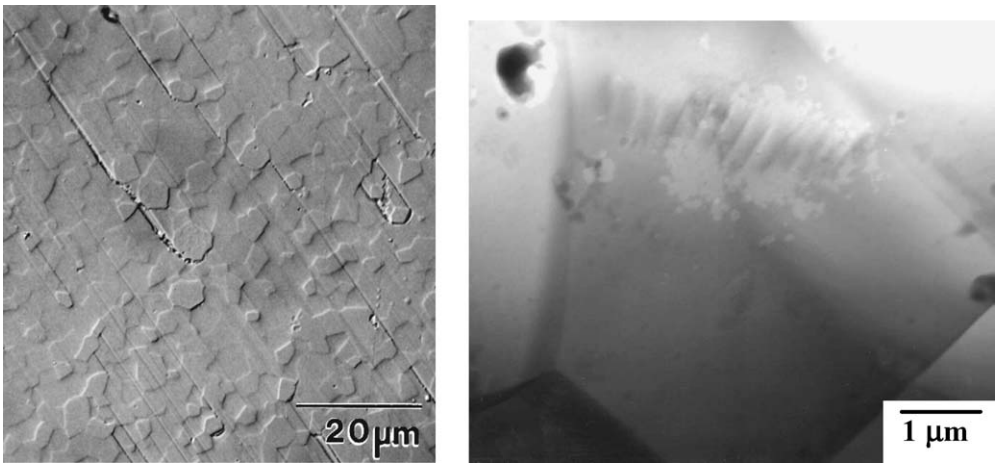

(a) (b)

Figure 4 (a) Nomarski optical micrograph of worn alumina, worn under water lubricated sliding, under the conditions given in Fig. 1. (b) TEM bright field image from a back-thinned sample, showing a region where the surface amorphous film has become detached. After [13].

change from mild wear to fracture dominated wear. Hsu and co-workers [6–8] provide useful wear transition maps, which allow the effect of load and speed to be accounted for. For alumina this transition is time dependent as well as load and speed dependent, Fig. 5. The transition, which is associated with 1–2 orders of magnitude increase in specific wear rate [13], involves a change from mild wear to intergranular fracture. Fig. 6a gives an SEM image of the post transition wear surface of a laboratory generated specimen (the same sample as in the dry wear test in Fig. 5). This can be compared with the explanted Al_2O_3 femoral head in Fig. 6b, which has failed due to post transition wear behaviour.

The transition is strongly grain size dependent, with the time to the transition decreasing with grain size. Modelling this transition, firstly by Cho *et al.* [14, 15] and later by Liu and Fine [19] and then Wang and Hsu [27, 28], has demonstrated that the grain size effect can be predicted by considering the combined effects of the contact stresses and the pre-existing thermal mismatch stresses (generated as a result of the anisotropy of thermal expansion coefficient in alumina) and a time dependent damage accumulation mechanism. Thus, the basic

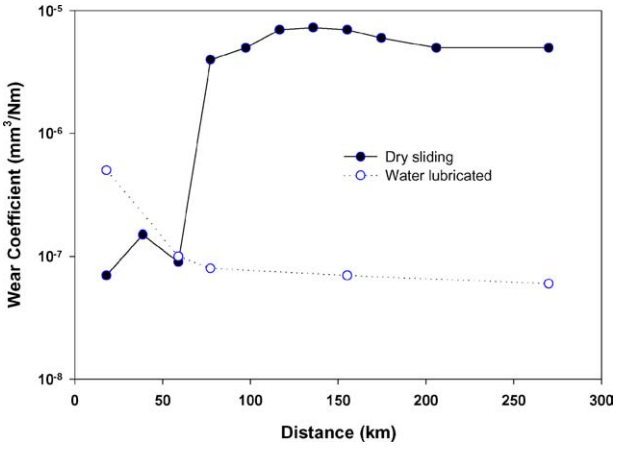

Figure 5 Wear coefficient as a function of sliding distance for alumina worn against Mg-PSZ showing the wear transition for dry sliding, but its absence for water lubricated sliding (during the 275 km test). After [13].

origin of the transition is well known, but the origin of the time dependent nature has received less attention.

Cho *et al.* [14, 15] have demonstrated extensive dislocation damage in the post transition regime. Barceinas-Sanchez and Rainforth [13] undertook a detailed investigation of the pre-transition regime, in particular, the time dependent damage accumulation mechanisms leading to the wear transition. Fig. 7 gives AFM images from the alumina pin worn in water in the pre-transition regime as shown Fig. 4a. The surface roughness and specific wear rate place this firmly within the mild wear regime. The worn surface in Fig. 4a shows several fine (0.3–1.9 μm diameter) abrasive grooves, which generally start at a grain boundary, frequently between grains that show the greatest height difference (i.e., it is usually associated with the grain boundary adjacent to a grain that has worn the least). An example of a back-thinned TEM micrograph from one such groove is given in Fig. 8. The damage fell into roughly four categories, grooves that predominantly produced fracture, grooves that predominantly produced dislocation damage, grooves that had both fracture and high dislocation density and finally grooves that apparently left no damage (the latter have been discussed previously under mild wear and shown in Fig. 4b). Which type of damage occurred strongly depended on crystallographic orientation, as shown by the dramatic change in damage that occurred from one grain to another, as shown by both the AFM (Fig. 7) and TEM (Fig. 8b and c).

The sample examined was just before the wear transition (as determined by a prior test under identical test conditions). As shown in Fig. 8d, some of the grain boundaries were cracked. Since the wear transition is associated with intergranular fracture, it is reasonable to assume that these cracks are the nuclei that lead to the wear transition. In all cases where such cracks were observed, dislocation pile-ups were present at the grain boundary. It is well known that such pile-ups can initiate cleavage fracture in metals, and therefore it is reasonable to consider that the grain boundary cracks occurred because of the combined effects of the applied stress at asperity contacts, the thermal mismatch stresses and

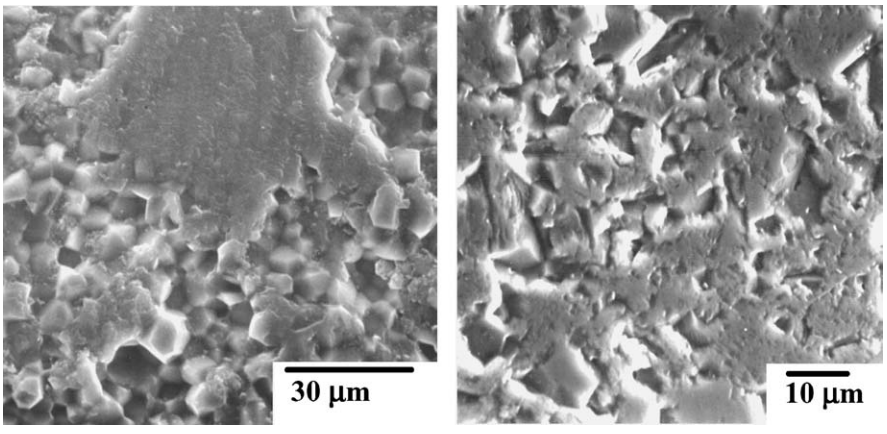

(a) (b)

Figure 6 SEM micrographs of worn alumina surfaces, operating in the post transition wear regime and exhibiting intergranular fracture. (a) The laboratory specimen, taken from the dry test show in Fig. 5; (b) Explanted alumina femoral head that failed due to excessive wear. (a) after [13], (b) after [25].

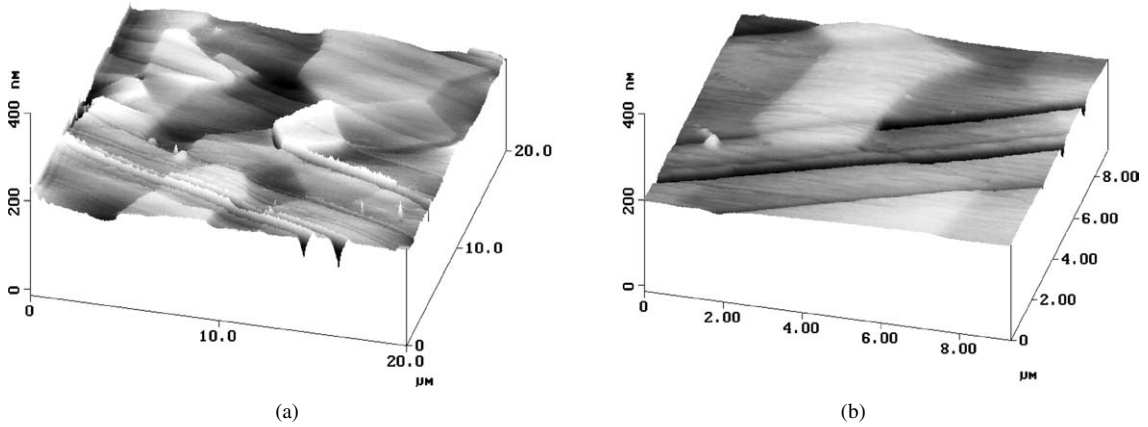

(a) (b)

Figure 7 AFM images from the worn surface shown in Fig. 4a. The maximum height difference in (a) is 33 nm. Note the manner in which micro-abrasive grooves initiate at the leading edge of a grain (leading edge is to the left of this image). Note the way in which groove depth changes from grain to grain, a particularly marked example of which is given in (b). After [13].

the elastic strain associated with the dislocation pile-up. The time dependent effect then arises from the build up of dislocation damage. The grain size effect results from both the scaling of thermal mismatch stresses with grain size, but also the increase in slip length and therefore dislocation density with grain size.

The Nomarksi contrast image of the worn alumina surface given in Fig. 4a, and the AFM images in Fig. 7, of the same surface, shows marked differential wear between grains, i.e., the wear rate appears to be dependent on the crystallographic orientation of the alumina. AFM demonstrated that the maximum surface relief was only ∼33 nm, with most changes in grain height being only 10–15 nm. The extent of grain relief depends strongly on the environment, and is not seen, for example, with a butanol lubricant, and not observed for the explanted alumina femoral head in Fig. 3b. Thus, the grain relief must depend, at least in part, on the absorption of the environment into the surface region. The origin of the grain relief is still not fully understood. Barceinas-Sanchez and Rainforth [13] plotted the grain orientation of surface grains on a stereographic projection, differentiating those grains that had worn more and those that had worn the least. No clear correlation could be found between crystallographic orientation and the grains that had worn the most. Interestingly, those grains that wore the most generally exhibited little or no evidence of dislocation damage and no microfracture. The only evidence of damage was the presence of a surface tribofilm, as already discussed, and illustrated in Fig. 4b. However, if only those grains standing proud of the surface are considered (i.e., those grains that had worn the least), the surface of the grain was between 70 and 78° to the *c*-axis of the crystal. Thus, this suggests that grains oriented for pyramidal slip would tend to wear less, i.e., in this specific respect surface plasticity appears to be beneficial.

Although there are a number of observations of dislocations at the worn surface, there are only a few detailed studies, namely those of Inkson [63], Hockey [16, 17] and Barceinas and Rainforth [13]. However, most studies have been concerned with abrasion or grinding. A detailed analysis of the dislocation activity *in the mild wear regime* yields interesting observations. Referring again to Fig. 8, while most dislocation activity was associated with these grooves, other dislocation activity was found at the worn surface, the majority of which coincided with the grains that wore the least. The dominant slip systems were pyramidal, namely:

$$\{01\bar{1}2\}1/3\langle\bar{2}021\rangle;\quad \{2\bar{1}\bar{1}2\}\langle01\bar{1}0\rangle;\quad \{10\bar{1}1\}1/3\langle\bar{1}2\bar{1}0\rangle;$$
$$\{10\bar{1}1\}1/3\langle\bar{1}101\rangle;\quad \{2\bar{1}\bar{1}3\}1/3\langle\bar{1}101\rangle$$

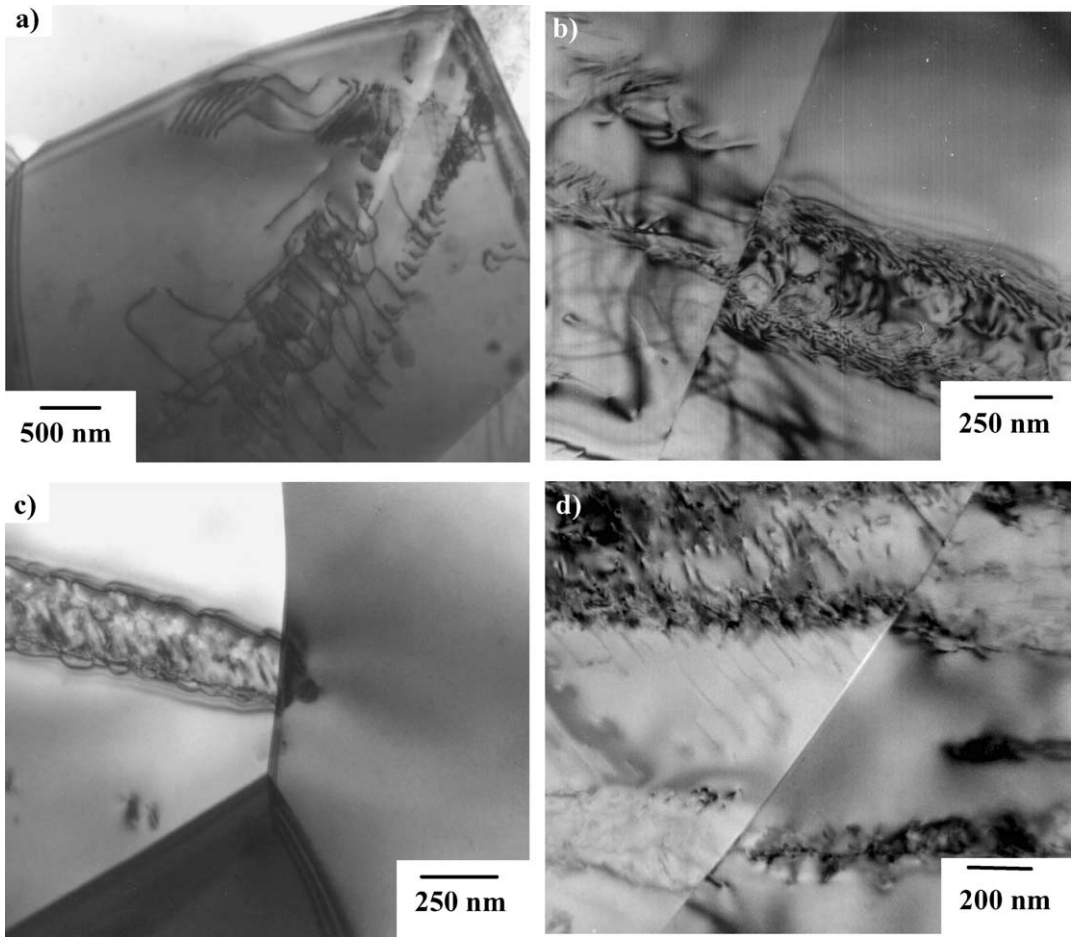

Figure 8 TEM bright field micrographs taken from a back-thinned sample of the surface shown in Fig. 7. (a) A groove showing extensive dislocation damage; (b) A groove where the damage is mainly fracture, but changes from one grain to the next; (c) A groove where there is no damage in a grain immediately adjacent to a deep groove; (d) grain boundary cracking associated with several pile-ups of dislocations. (b) and (c) taken from [13].

Occasional basal slip was also observed, of the type $(0001)1/3\ \langle 11\bar{2}0\rangle$. No evidence of prism slip was found. Table I gives the orientation of the slip system to the worn surface, from which it can be seen that the majority of pyramidal slip occurred on planes between ∼6–33° to worn surface, although three examples of slip on planes ∼48–52° to the worn surface were also identified. Basal slip was occasionally found, with angles of ∼31° and ∼53–73° to the worn surface. Basal twinning was also present in association with basal slip, with a twin fault vector of $1/3\ \langle\bar{1}2\bar{1}0\rangle$ associated with the Burgers vector of the basal dislocations was of the type $1/3\ \langle 11\bar{2}0\rangle$. No evidence of rhombohedral twinning was found anywhere on the worn surface.

TABLE I Table of the angle between the slip plane and the worn surface (ϕ) and the slip direction and the worn surface (λ), for some of the grains in which the slip system was quantified

Grain surface normal	Slip plane	Burgers vector	ϕ	λ
$[\overline{92}\ 16\ 76\ \overline{93}]$	$(0\ 0\ 0\ \bar{1})$	$1/3[\bar{2}\ 1\ 1\ 0\ ]$	30.7°	61.4°
$[29\ \overline{16}\ \overline{13}\ 12]$	$(0\ 0\ 0\ 1)$	$1/3[\ 2\ \bar{1}\ \bar{1}\ 0]$	53.1°	36.4°
$[20\ \overline{55}\ 35\ 18]$	$(1\ \bar{1}\ 0\ 2)$	$1/3[\ 0\ \bar{2}\ 2\ \bar{1}\ ]$	33.1°	70.3°
$[\bar{3}\ 9\ \bar{6}\ \bar{4}]$	$(\bar{1}\ 2\ \bar{1}\ \bar{2})$	$[\ 1\ 0\ \bar{1}\ 0]$	20.5°	81.4°
$[\bar{6}\ 3\ 3\ 1]^{a}$	$(0\ 0\ 0\ 1)$	$1/3[\bar{2}\ 1\ 1\ 0]$	73.2°	16.5°
$[\overline{29}\ 31\ \bar{2}\ 6]^{a}$	$(0\ 0\ 0\ 1)$	$1/3[\bar{1}\ 2\ \bar{1}\ 0\ ]$	72.6°	31.3°
$[\overline{17}\ 13\ 4\ 3]^{b}$	$(\bar{2}\ 1\ 1\ 2)$	$[\ 0\ 1\ \bar{1}\ 0\ ]$	16.4°	73.7°
$[\overline{17}\ 13\ 4\ 3]^{b}$	$(\bar{1}\ 1\ 0\ 1)$	$1/3[\bar{1}\ \bar{1}\ 2\ 0\ ]$	12.4°	77.5°
$[\overline{17}\ 13\ 4\ 3]^{b}$	$(\bar{1}\ 1\ 0\ 1)$	$1/3[\bar{1}\ 0\ 1\ \bar{1}\ ]$	12.4°	83.4°
$[\bar{5}\ 3\ 2\ 1]^{b}$	$(\bar{2}\ 1\ 1\ 2)$	$[0\ 1\ \bar{1}\ 0]$	6.2°	83.7°
$[46\ \overline{29}\ \overline{17}\ 6]^{b}$	$(1\ \bar{1}\ 0\ 1)$	$1/3[\ 1\ 1\ \bar{2}\ 0]$	21.1°	69.1°
$[46\ \overline{29}\ \overline{17}\ 6]^{b}$	$(1\bar{1}\ 0\ 1)$	$1/3[1\ 0\ \bar{1}\ \bar{1}\ ]$	21.1°	76.8°

[a]Grains standing proud of the surface.
[b]Plane also contained basal twins.

Although the slip systems noted above have been previously observed in bulk compression studies [20], there are important differences to the current results. Lagerloff *et al.* [20] collated yield stress data from bulk compression testing over a wide temperature range, and found that pyramidal slip is the *least* favoured at all stresses and temperatures, whereas in the work of Barceinas and Rainforth, it was the most dominant slip system. For example, at 100°C prism slip would be expected to be dominant, with a yield stress of ∼7 GPa. Conversely, basal slip would be expected at 1100°C with a yield stress of ∼180 MPa.

These findings also contrast the observations of Hockey [16, 17], who found that for sapphire, basal slip dominated under an indentation and under abrasive grooves induced by 0.25 μm diamond. Indeed, basal slip was predominant even when the basal surface was indented, although he identified limited $\{11\bar{2}\ 3\}\{\bar{1}012\}$ and $\{10\bar{1}1\}$ pyramidal slip under microhardness indents on other sapphire surface orientations. However, Inkson [63] recently undertook a detailed analysis of the abrasion of sapphire by diamond and found deformation was predominantly by basal twinning and pyramidal

slip ($1/3\langle 11\bar{2}0\rangle\{\bar{1}101\}$). Thus, Inkson's observations on abrasion are consistent with the work of Barceinas-Sanchez and Rainforth on sliding wear, both of which show a marked shift in glide plane of $1/3\langle 11\bar{2}0\rangle$ from basal to pyramidal. Interestingly all three studies failed to observe prism slip. Therefore, the available wear surface data suggests that similar slip systems are activated by asperity contact, but differ in a major way to bulk compression tests.

A number of factors could explain these apparent anomalies [13]. Firstly, the strain rate at the absolute surface during wear (estimated [13] as $\dot{\varepsilon} \sim 10^5\ s^{-1}$) is substantially higher than used in bulk compression studies [20], and most critically resolved shear stresses are strain rate dependent. Secondly, it is known that dislocation activity at a surface can be significantly different to that in the bulk [13], although such evidence comes largely from metals, not ceramics. Thirdly, and perhaps most significantly, the surface plasticity will have been altered by the adsorption of water. The environment is known to strongly affect surface plasticity and fracture [13, 33, 35, 36].

The role of plastic deformation in the wear of ceramic materials remains controversial, largely because of the paucity of data. Surface plasticity is often invoked to explain SEM micrographs which indicate a 'smearing' of the surface, but a qualitative description is dangerous. Such surface smearing is usually associated with the formation of a 'tribo-layer' which is essentially an agglomeration of very fine wear particles [2]. For alumina and other similar ceramic materials, it is not possible to get gross surface plasticity. Nevertheless, dislocation flow can play a major role, as shown by the time dependent effect.

5. Strategies for extending the mild wear regime in ceramics without transformation toughening

Since the initial work of Niihara [40–42], the superior mechanical properties of ceramic nanocomposites, in particular Al_2O_3-SiC, have been extensively investigated (although the term 'nanocomposite' is perhaps a misnomer here, since the alumina grain size remains firmly in the micron range, while the SiC particles are tens of nm, often larger). While some of the original claims for the mechanical properties of Al_2O_3-SiC have been the subject of much controversy, it is clear that these materials offer significant benefits in wear behaviour compared to monolithic Al_2O_3. Erosive and abrasive wear rates are substantially reduced by the addition of SiC [43–54]. For example, nanocomposites tend to exhibit a surface covered in plastic deformation grooves, while for the same conditions, the monolith exhibits intergranular fracture. Consequently, the nanocomposites are much easier to polish.

The understanding of the underlying mechanisms in the wear of Al_2O_3-SiC composites is most complete for abrasion. Wu *et al.* [52] have undertaken a detailed investigation of the residual stresses at the surface of ground Al_2O_3-SiC and Al_2O_3 using Hertzian indentation, and showed a larger compressive residual stress in the composites compared to the monolith. For the composite, this residual stress was measured at 1500 MPa, in the near surface regions for the polished condition. Fracture toughness values, also determined by the Hertzian indentation method, were higher for the composites than the monolith.

The residual stresses in the nanocomposite were correlated by Wu *et al.* [52] with the presence of regions of high residual dislocation density in the near surface regions. The comparison with the monolith depended on the abrasion conditions, i.e., the grit size used. For the initial ground condition, intergranular fracture of the alumina dominated, and therefore much of the deformed surface was lost. Where it remained, deformation was dominated by twinning, although some dislocation damage was also observed. In contrast, the nanocomposite exhibited only dislocation glide, with no evidence of twinning. While the differences were marked, it should be remembered that more material will have been lost from the alumina surface compared to the composite, and therefore more of the evidence of deformation mechanisms will also have been lost. In the polished condition for a grit size of 3 μm or finer, dislocation flow was observed for both materials in a small surface region, being confined to the surface grains for the nanocomposites. Importantly, even for these grit sizes, the depth of the deformation zone was much greater for the nanocomposites than for the monolith.

This observation was later confirmed by Wu *et al.* [54] who used FIB and TEM to examine the surface of similar materials. In their work, the depth of deformation below a 120° cone indenter was $\sim$7 μm for an Al_2O_3-5%SiC composite, while it was $\sim$4 μm in the alumina. Importantly, the deformation was constrained to the first layer of grains for the alumina, but extended to several grain depths for the composite. These authors used multiple FIB cuts to image the crack distribution below the surface, as shown in Fig. 9. They then reconstructed the images to give a 3-D image of the crack distribution, Fig. 10. Interestingly, the crack distribution was similar for both materials, with cracking extending >7 μm below the bottom of the scratch, and >10 μm from the centre line of the scratch track for both cases, even though the deformation behaviour was quite different. In line with Wu *et al.*, the residual stresses were greater for the nanocomposite than the monolith, consistent with the different levels of deformation.

Wear studies of ceramic nanocomposites have not explicitly examined the wear behaviour in relation to the wear transition [56]. In abrasion and erosion studies, the nanocomposite has been compared to the monolith, but under conditions where the monolith is clearly operating post-transition, as shown by the intergranular fracture. While this shows that the nanocomposites are certainly less susceptible to a wear transition from gross surface fracture, it does not explicitly show that a wear transition does not occur for the nanocomposites. In these studies, the greater resistance to intergranular fracture has been ascribed to two factors. Firstly, the modification of inherent grain boundary strength could

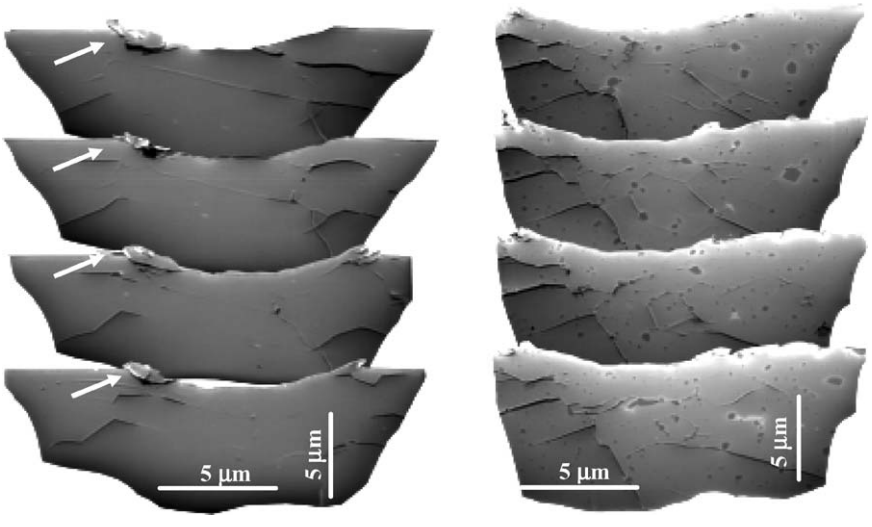

(a) (b)

Figure 9 After Examples of multiple parallel 2D FIB cross-sections (spacing schematic) showing subsurface fracture damage under the scratch grooves in (a) Al_2O_3, (b) Al_2O_3/5vol.% nanocomposite. The viewing angle is 45° from the milled plane. The arrow indicates limited pile-up of material above the original surface height at the scratch groove edges. After [54].

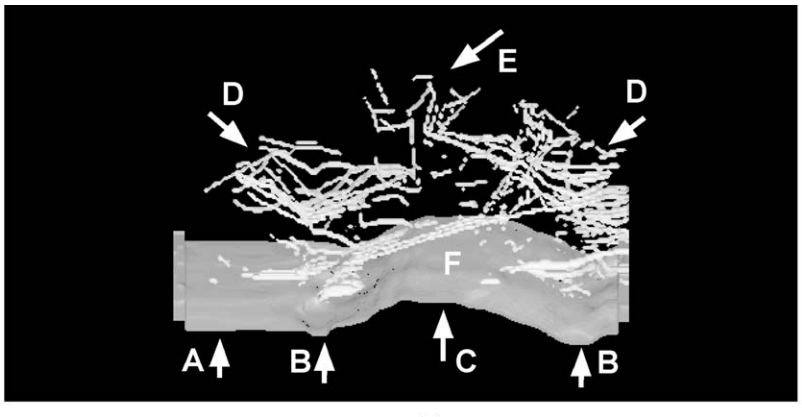

(a)

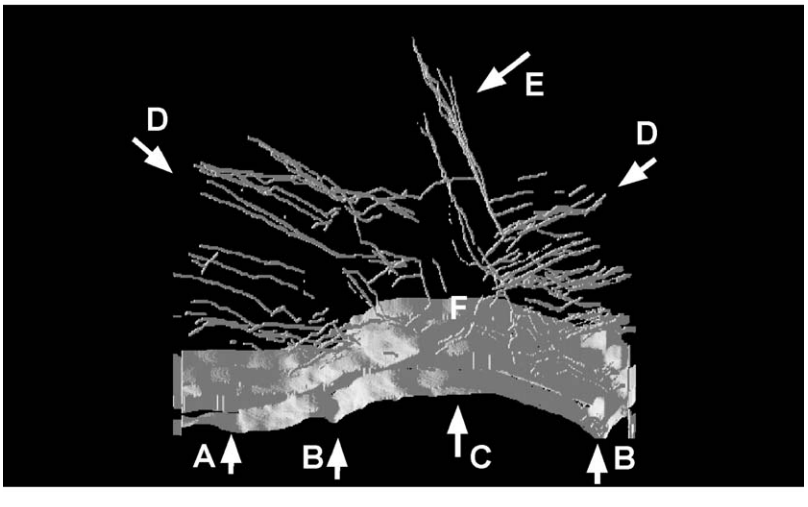

(b)

Figure 10 3D reconstructions of the crack morphologies around a 1 N load scratch track (solid surface at the bottom of each image), viewed "inverted" from inside the sample. The scratch track is shown in grey, with the cracks white on a black free space background. (a) Polycrystalline alumina: reconstructed dimension 19.1 μm across scratch $\times$7.2 μm along scratch. (b) Polycrystalline Al_2O_3/5vol.% nanocomposite: reconstructed dimension 16.8 μm across scratch $\times$4.3 μm along scratch. Residual cracks around the scratch site penetrate more than 7 μm into sample from groove bottom in (a) and more than 10 μm in (b). Taken from [54].

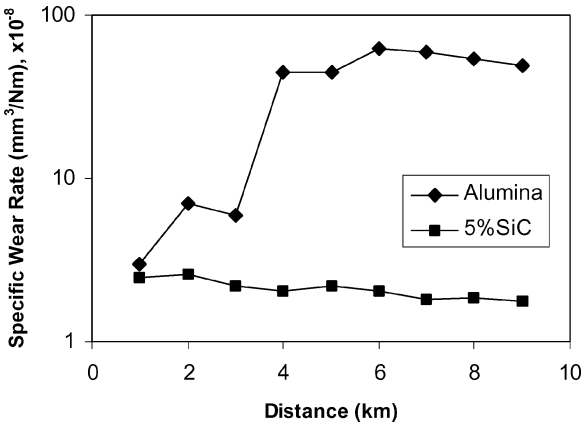

Figure 11 Specific wear rate as a function of sliding distance for monolithic alumina and alumina +5%SiC, for a load of 60 N. The monolith exhibits a wear transition, while the composite does not. After Bajwa [61].

remove the catastrophic nature of surface damage associated with intergranular fracture that is responsible for the transition. Secondly, the change in dislocation density and residual stress-state in the composite compared with the monolith could alter the time dependant nature of the damage accumulation process.

Fig. 11 gives sliding wear data comparing the behaviour of monolithic alumina with the nanocomposite under near identical test conditions. The monolith shows a time dependent wear transition, while the nanocomposite does not. Note, however, that the specific wear rates are similar in the early part of the test, i.e., in the pre-transition regime for the monolith, implying that the addition of SiC does not significantly modify the wear rate in the mild wear regime. Fig. 12 gives wear data taken from Chen *et al.* [56], which shows that it is not the grain size which is primarily responsible for removing (or delaying) the wear transition, further supporting the view described above, that it is the strengthening of the grain boundaries that has the principal role.

Fig. 13 shows the worn surface of a nanocomposite, tested under conditions that yielded immediate post transition behaviour in the monolith. Macroscopically the surface was smooth, while there was some evidence of fine-scale abrasion at the microscopic scale. Fig. 14 gives bright field TEM images from a back thinned worn surface of the same material. There is extensive dislocation activity associated with the region under the grooves (i.e., those seen in Fig. 13). The dislocation activity was essentially similar to that observed by Barceinas-Sanchez and Rainforth [13], as shown in Fig. 8, with a few important exceptions. Firstly, the dislocation density was generally higher than for the monolith. The dislocation density was more homogeneous between grains, with dislocations generally restricted to regions below the abrasive grooves, with no evidence of dislocation pile-ups at grain boundaries. Finally, there was no evidence of grain boundary cracking. Interestingly, the dislocation activity did not appear to be perturbed by the SiC (i.e., there was no evidence of the dislocations interacting with the residual stress field around SiC particles). Thus, although the data in Figs. 11 and 12 does not determine definitively whether the time dependent wear transition is removed by the addition of fine SiC to Al_2O_3, or merely delayed to long times, this TEM evidence strongly suggests that there is no time dependent transition for these materials.

There remains little agreement regarding the origin of the much more extensive dislocation activity in the surfaces of the nanocomposites, but whatever mechanism is proposed, it has to be consistent with the similar hardness and stiffness values of the two materials. Wu *et al.* [52] propose a number of possibilities: (a) The large thermal expansion coefficient mismatch between the two phases ($\sim 8 \times 10^{-6}$ K^{-1} for Al_2O_3 and $\sim 3 \times 10^{-6}$ K^{-1} for SiC) potentially results in dislocations punching out into the matrix during cooling; (b) as for (a), but the thermal mismatch results in residual elastic strains. These aid deformation by superposition of the applied stress, i.e., a mechanism similar to the well known thermal cycle plasticity in hexagonal metal; (c) as noted above, the greater removal rates in the alumina by intergranular fracture result in material loss before deformation can be established. Wu *et al.* rejected (b) since similar elastic strains would be found in conventional Al_2O_3-SiC composites (as opposed to 'nanocomposites'), but such materials do not show the enhanced plastic deformation. The FIB work of Wu *et al.* [54] demonstrated that dislocations were activated at both the surface and at the interface between Al_2O_3 and SiC, which is inconsistent with (a), which implies it is the pre-existing dislocation density that is

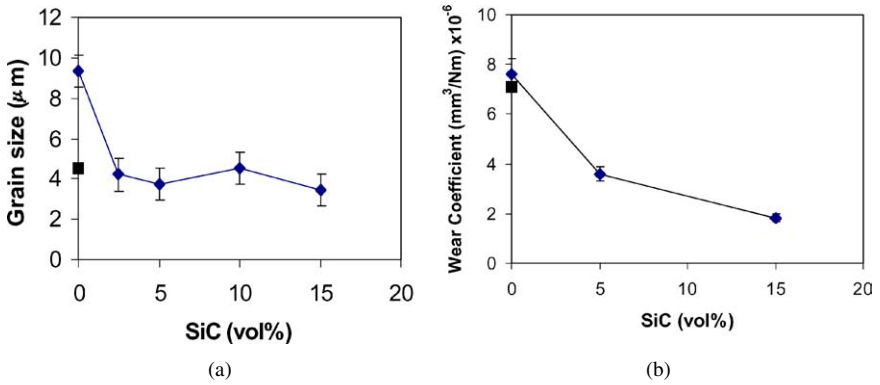

Figure 12 (a) Grain size as a function of SiC content (♦ data series, ■ additional monolithic material processed to have finer grain size); (b) Wear coefficient as a function of SiC addition for the materials with grain sizes detailed in (a). After Chen *et al.* [56].

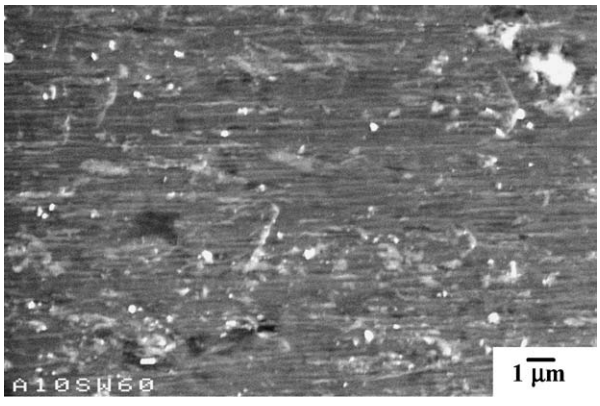

Figure 13 Secondary electron SEM image of the worn surface of the Al_2O_3-10%SiC tested under a load of 60 N. Note the fine abrasive grooves. After Bajwa [61].

important. However, there remains no direct evidence as to whether (a) or (c), or a combination of both, can adequately explain the substantially enhanced dislocation activity found for the Al_2O_3-SiC nanocomposites.

6. Wear in transformation toughened zirconia

Many workers have highlighted the importance of fracture toughness in the wear of ceramics [4], promoted by the controlled phase transformation of metastable tetragonal zirconia (hereafter t-ZrO_2) to monoclinic zirconia (hereafter m-ZrO_2), with the associated volume expansion. Zirconia ceramics offer the highest toughness of all monolithic ceramics, but also exhibit high hardness and good resistance to chemical attack. Therefore, in principal, these materials should provide excellent wear resistance. However, the published literature provides conflicting information. Some reports indicate that zirconia ceramics have good wear resistance both in the laboratory [68–70] in field trials [71–73], while others workers have found poor wear resistance [62, 74–77], even under mild sliding conditions.

The role of transformation toughening in the wear of zirconia ceramics remains controversial. Zirconia ceramics offer greater resistance to grinding than would be expected from the hardness, and it is generally agreed that this is a result of the surface compressive stresses generated by transformation of the t-ZrO_2 to m-ZrO_2 [4], with evidence for this coming from X-ray diffraction. In contrast, sliding wear rates are generally higher than expected from the hardness [62, 79, 80]. There are a wide range of explanations for this, for example, this has been ascribed to surface fracture initiated by transformation-induced microcracking [76], but also to the poor thermal conductivity of zirconia that results in substantial temperature rises at the surface, thus softening the material [66]. The discussion below takes a critical look at the poor wear performance of these materials and tries to explain the apparent anomalies in behaviour.

The wear rate of zirconia is found to be bad in water as well as under dry sliding conditions [5, 82]. This is in contrast to some other ceramics such as alumina [13], where water lubrication can reduce the wear rate by orders of magnitude. Water lubrication should reduce the heat input and contact stresses and therefore the wear rate, but this is not the case for zirconia. This has led to suggestions that hydrothermal degradation occurs during sliding and the high wear rate in water results from the microcracking associated with the tetragonal to monoclinic transformation [76] (there is not space here to discuss hydrothermal degradation, the reader is referred to [89] for a review. The term refers to the uncontrolled surface phase transformation of t-ZrO_2 to m-ZrO_2, with kinetics that peak in the temperature range $\sim$150–250°C and is accelerated by the presence of water. It generally results in a catastrophic loss in mechanical properties).

Fig. 15 shows the worn surface of a 3 mol% TZP worn against a zirconia toughened alumina counterface [66] under conditions (0.24 m/s, 19 N) that have yielded mild wear for many ceramic couples. However, the wear coefficient of the zirconia (1.8×10^{-4} mm^3/Nm) was excessive, and the test was associated with significant noise and vibration. Fig. 16 gives bright field TEM

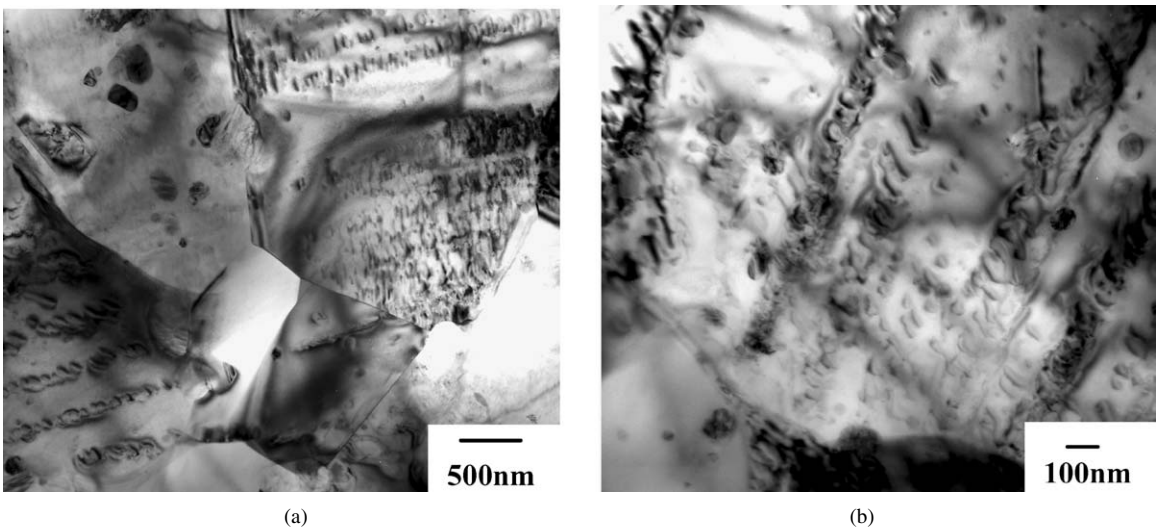

(a) (b)

Figure 14 Bright field TEM micrographs from back-thinned samples of Al_2O_3-10%SiC. (a) General view, showing dislocation contrast associated with fine abrasive grooves. (b) Higher magnification image showing apparently minimal interaction between dislocations and SiC particles. After Bajwa [61].

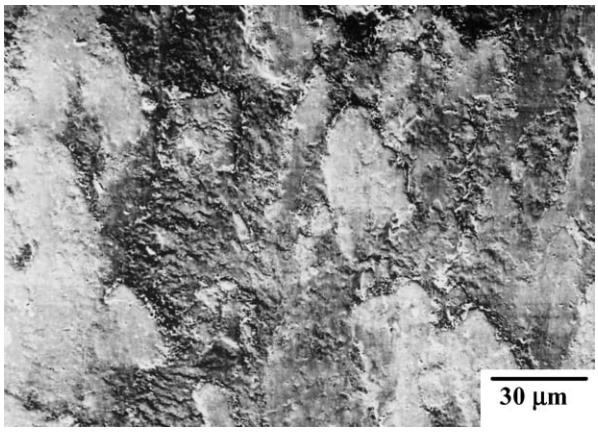

Figure 15 Backscattered electron SEM micrograph of a worn 3Y-TZP, tested in dry sliding against a zirconia toughened alumina counterface, at 19 N and 0.24 m/s. The darker regions are rich in Al^{3+}. After [66].

images from a longitudinal cross-sectional specimen of this test. The micrographs in Fig. 16a show three broad categories, labelled A, B & C on Fig. 14a. The starting microstructure was of equiaxed tetragonal zirconia grains with an average grain size of ~0.6 μm. Region A comprised elongated tetragonal zirconia grains, with a maximum aspect ratio of 30:1, equivalent to a true tensile strain of 1.7 (Fig. 16b). The elongated grains contained a high dislocation density. Region B contained fine (~50 nm) equiaxed tetragonal zirconia grains, with extensive grain boundary cracking. This represents an order of magnitude reduction in microstructural scale from the starting material. Region C, Fig. 16c, was predominantly amorphous, containing approximately equal proportions of Al and Zr ions, but also containing fine (~5 nm) zirconia precipitates and fractured alumina particles.

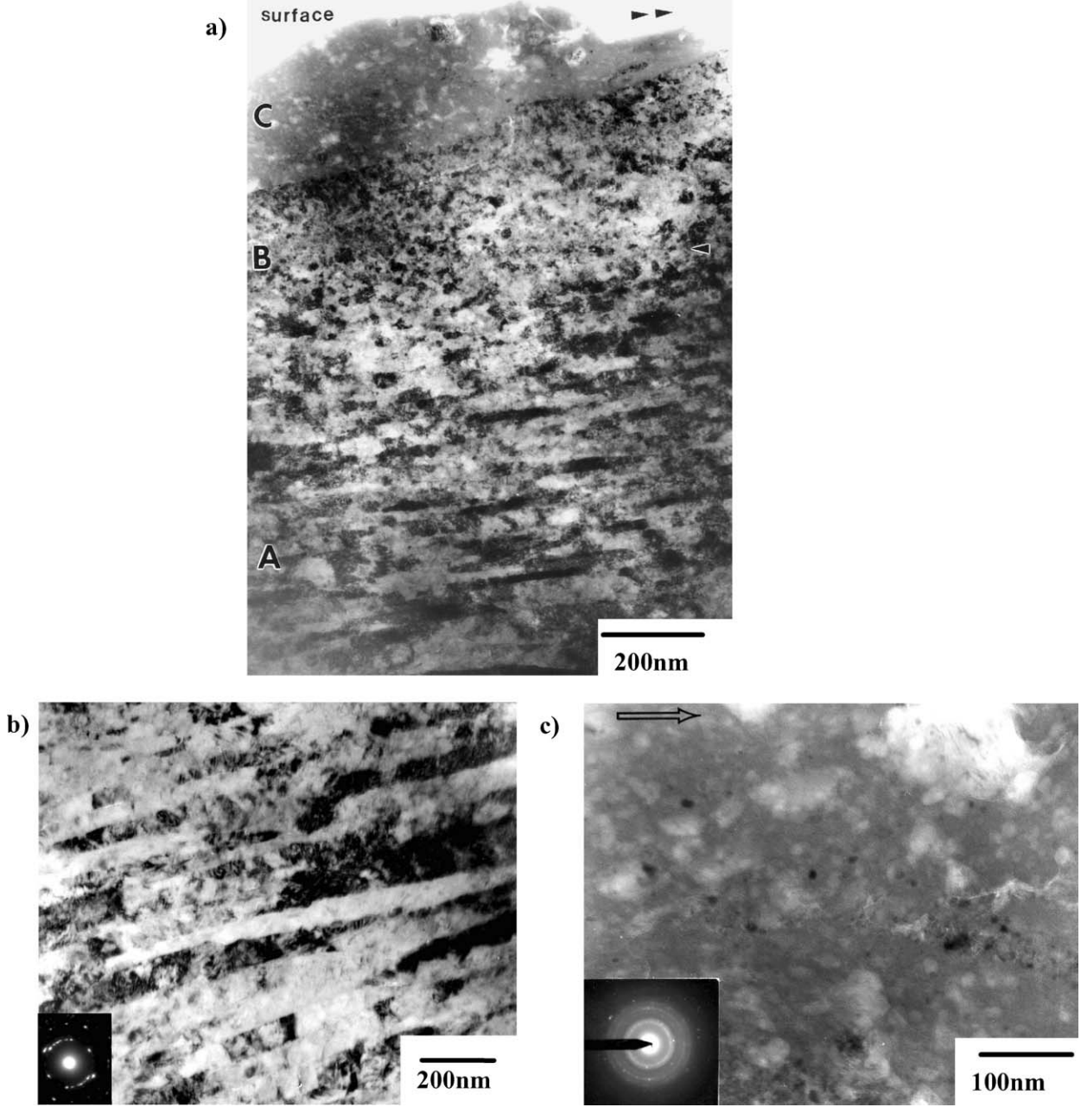

Figure 16 Bright field TEM micrographs from a longitudinal cross-sectional sample of the worn surface shown in Fig. 15. (a) Overview, which contains 3 principal regions, A, B and C, discussed in the text; (b) Enlarged image of region B, showing severe plastic deformation of the t-ZrO_2 grains; (c) Enlarged image of region C showing fragmented alumina particles (light regions) and a matrix which is partly amorphous and partly nanocrystalline and contains both Zr and Al ions. After [66].

The origin of the high strain deformation in the zirconia and the substantial reduction in crystallite size is complex and discussed in detail elsewhere [66]. However, the microstructural changes can only be explained by high flash temperatures generated as a result of the low thermal conductivity of the zirconia. Estimation of the flash temperatures induced at the surface by the friction forces is difficult, because they are localised and temperature transients occur over short times. Experimental methods, such as implanted thermocouples, do not register the localised flash temperatures. Estimates of surface temperature can be made from analytical models, for example, Ashby and co-workers [9], have calculated flash temperature maps for a wide range of experimental conditions. Using this analysis, Woydt *et al.* [65] calculated the flash temperature rise over a wide range of speed and load conditions for zirconia. For the test shown in Fig. 16, this suggests a rise of ∼800°C at the surface, assuming a total contact area of 0.1 mm^2. As with every calculation of flash temperature, it is the estimate of true contact area that is a problem, and the value of 800°C is rather low to explain microstructures presented in Fig. 16, suggesting a smaller true contact area in this case.

The gross plastic deformation shown in Fig. 16 was the first observation of high strain deformation in a ceramic resulting from dislocation flow, but it is believed to be an observation which is restricted to cases where a substantial temperature rise occurs during frictional contact, such as zirconia ceramics (further work is required to confirm this). The only other examples of significant dislocation activity at worn surfaces are in the ceramic nanocomposites, as already discussed before, but in this case, no grain shape change occurred.

The outer layer, region C, is a true mechanically mixed layer, as often observed in the wear of metal on metal systems [90]. The mechanism by which an amorphous mixture of alumina and zirconia can form is not clear, but is believed to result from solid state amorphisation, since temperatures did not appear to be high enough for liquation of the surface. Solid state amorphisation generally follows a sequence of a continuous decrease in crystallite size, diffusional mixing of the two components, ultimately leading to a loss of the crystal structure [52]. The issues are discussed in more detail in reference [34].

It is clear from the above that even under mild sliding conditions, the low thermal conductivity of zirconia results is substantial temperature rises. Indeed, it is becoming increasingly apparent that the wear of zirconia is dominated by flash temperature rises. An elegant demonstration of this is the work of Woydt and coworkers [64, 65, 81]. Woydt and Habig [16] and Woydt *et al.* [81] have demonstrated that the wear rate of zirconia depends sensitively on the sliding speed and test temperature, with the wear rate increasing by 4 orders of magnitude for an increase in sliding speed from 0.003 to 1 m/s. Indeed, Fig. 17 gives a plot of specific wear rate as a function of sliding speed using data from the literature, which clearly demonstrates the dominant effect of sliding speed. The combination of this, and the TEM results given in Fig. 16 strongly suggests that transformation of tetragonal to monoclinic zirconia is not a significant mechanism except where frictional heating is minimised, i.e., at very slow sliding speeds (<0.01 m/s).

As noted earlier, the observation that wear rates do not decrease with water lubrication has been explained by the presence of hydrothermal degradation, i.e., the water was acting to promote unstable t-ZrO_2 to m-ZrO_2 transformation at the surface. Barceinas-Sanchez and Rainforth [83] examined this hypothesis by comparing the surface structures developed under dry and water lubricated sliding, for otherwise identical test conditions (3Y-TZP, against an Mg-PSZ at 10 N load and 0.24 m/s). High wear rates were recorded for both tests (dry: $6.8\times10^{-4}mm^3/Nm$, wet: $2.2\times10^{-4}mm^3/Nm$). Interestingly, both surfaces exhibited the same features, although the extent of each particular attribute differed slightly. Fig. 18a shows the extreme outer ∼400 nm of the water lubricated test, which consisted of randomly oriented, fine (∼8 nm) tetragonal/cubic

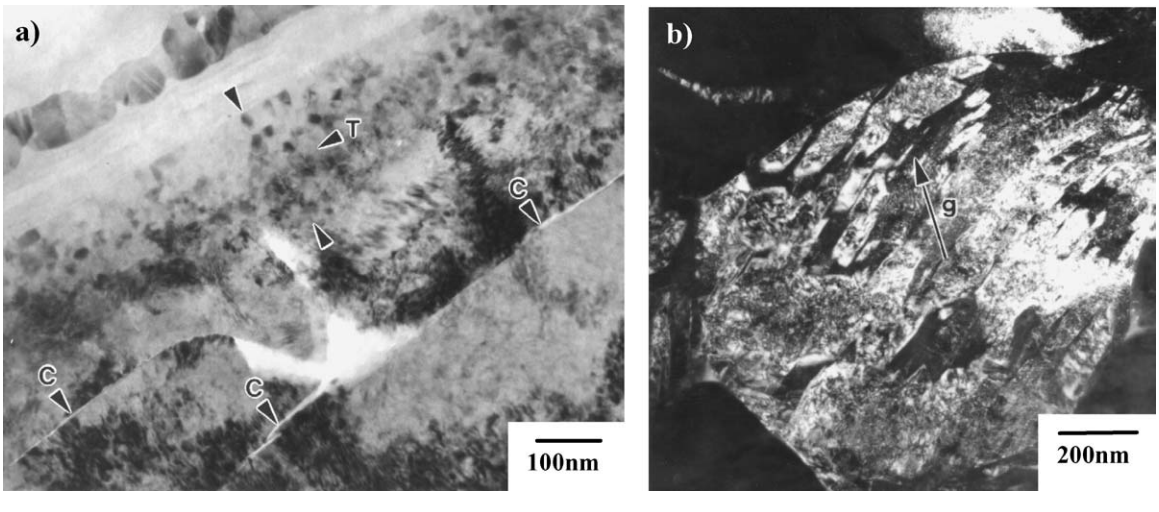

Figure 17 TEM micrographs from a longitudinal cross-sectional sample of a worn sample worn under identical conditions to that shown in Fig. 16, but with water lubrication. (a) Bright field image of the near surface region, which comprised a nanocrystalline t-ZrO_2 layer (marked 'T'), with elongated t-ZrO_2 grains just below, and grain boundary cracking (marked 'c'); (b) Dark field image of a region approximately 1.5 μm from the worn surface, showing a grain which has monoclinic symmetry. Note the plastic deformation of this phase in the upper region of the grain. After [83].

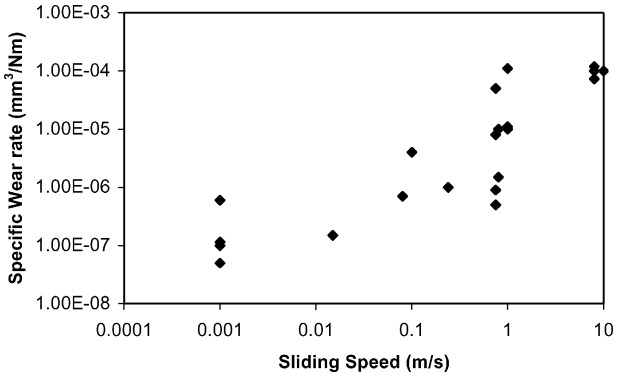

Figure 18 Specific wear rate as a function of sliding speed with the data taken from the literature for a variety of test conditions.

zirconia crystals. As with the earlier results of Rainforth and Stevens [62], extensive deformation of the t-ZrO_2 grains by dislocation flow was observed. Transformation to monoclinic symmetry was found at a depth of 1.0–2.2 μm in the water lubricated test. Importantly, some of the m-ZrO_2 phase had been deformed in the direction of sliding, Fig. 18b. This indicated that stress induced transformation of t-ZrO_2 to m-ZrO_2 occurred well below the surface, where the temperature was low enough, followed by plastic deformation as the stress gradually increased on the m-ZrO_2layer, because of progressive wear of the surface (a point 3.5 μm below the surface, where the first microstructural change occurred, would become exposed to the surface by wear after ~150 s due to wear, undergoing a series of microstructural transformations in the process). Finally, the m-ZrO_2 re-transformed to t-ZrO_2, as the temperature rose within this layer as material removal from the surface occurred. This categorically places the temperature at least at ~560°C, which is the equilibrium transformation temperature on heating [4], (although the rapid heating associated with flash temperature rises would be expected to *increase* the phase transformation temperatures).

These results not only show that water provided little lubrication, as shown by the evidence of high surface temperatures, but also that a hydrothermal degradation mechanism did not occur for water lubricated tests. These observations are therefore likely to explain the restricted mild wear regime in the wear maps presented by Kato and Adachi [1], as discussed in Section 3.

Where the temperature rises are restricted there are examples where the t-ZrO_2 to m-ZrO_2 transformation does play an important role in the wear response of zirconias. Fig. 19a gives an SEM image of a worn Mg-PSZ, which had been in intermittent contact with a stainless steel counterface, where the heat generation was limited. Interestingly, the grain relief was observed, which shows many similarities with the alumina surfaces shown in Fig. 4a. In addition, pitting can be seen, that is clearly related to the crystallographic orientation of the grain. Similar observations have been made by, for example, Hannink *et al.* [72]. TEM, Fig. 19b, showed that the cracks occurred preferentially along {100} cubic planes, which was consistent with the twin variants of the m-ZrO_2 which were highly populated along $(001)_m$, so that maximum strain was generated

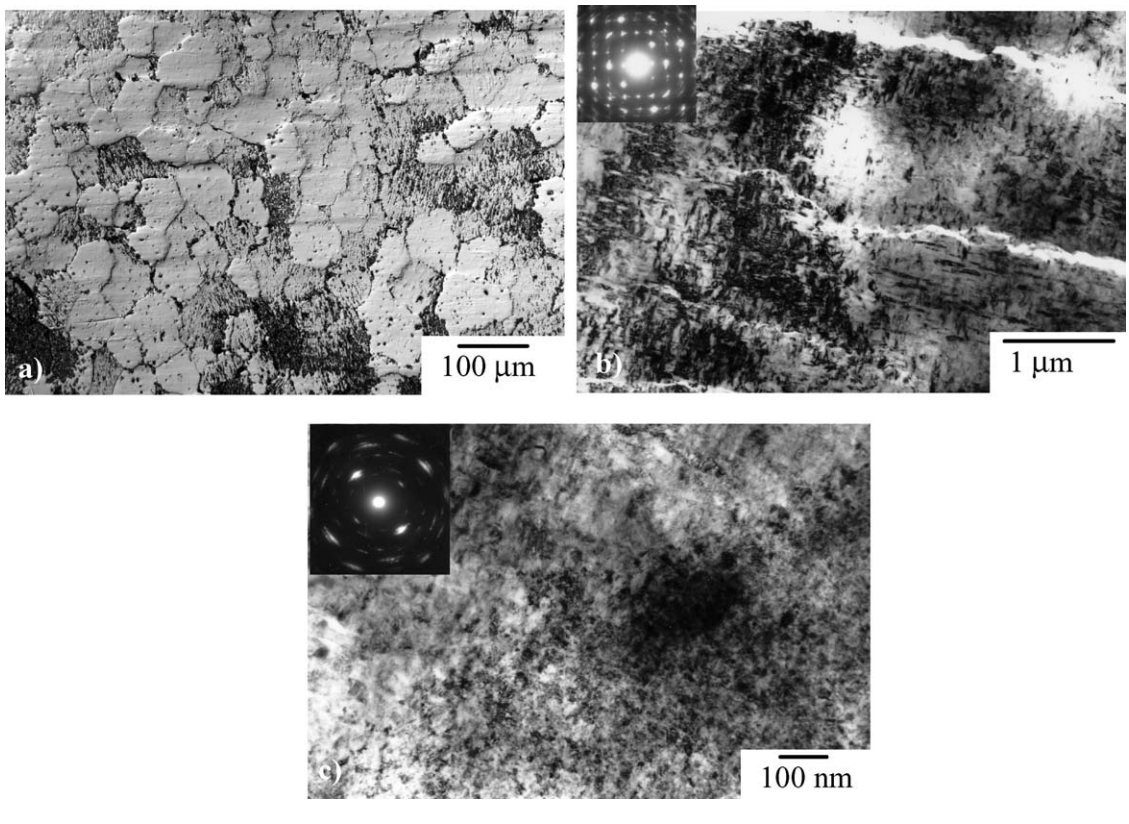

Figure 19 (a) Nomarksi contrast optical micrograph of a worn Mg-PSZ surface, after sliding against a 316 L stainless steel. Note the differential wear between grains; (b) Bright field TEM micrograph of a back-thinned sample, showing cracking along the [100] directions; (c) Bright field TEM micrograph of the same sample as (b), showing extensive plastic deformation below a fine abrasive groove. After [62].

along the [100] cubic directions. Thus, in this instance, the transformation of t-ZrO_2 precipitates to m-ZrO_2 was, at least in part, detrimental.

Interestingly, gross plastic deformation was also observed in this material below abrasive grooves, Fig. 19c. For the Mg-PSZ, this resulted in fragmentation of the t-ZrO_2 precipitates. While dislocations could not be identified, the significant arcing in diffraction rings clearly indicates some form of subgrain structure. Thus, the behaviour below the abrasive groove was qualitatively similar to that observed in monolithic Al_2O_3 and Al_2O_3-SiC nanocomposites. This observation contradicts the commonly held view that in grinding, the t-ZrO_2 transforms to m-ZrO_2 at the surface. This is based on XRD observations, which sample a depth of about 5 μm (for Cu K_α radiation), and therefore will not differentiate between the different layers observed, e.g., in Fig. 16 or 17. TEM results suggest that the extreme surface is made up of deformed t-ZrO_2, and the m-ZrO_2 is present as a layer below this. However, this is a detail, and the important point remains that the m-ZrO_2 layer infers compressive stresses that enhance the wear resistance.

7. Conclusions

1. There has been much useful development of wear maps, and contact severity parameters defined that allow the wear of ceramics to be mapped as a function of contact severity. This allows a clear definition of mild and severe wear that should be used universally in the literature. However, further work is required to introduce microstructural parameters into such modelling.

2. Operation of ceramics in the mild wear regime results in smoothing of the surface, by definition. However, microscale abrasion may still occur and differential wear may be observed between grains, demonstrating that wear rate can depend on crystallographic orientation. Although dislocation activity can occur below microscopic abrasive grooves, this localised plastic deformation is not believed to be rate limiting in mild wear. Rather, the predominant wear mechanism is believed to be tribochemical, with wear resulting in the formation of amorphous films.

3. The time dependent wear transition results from a combination of applied stress, residual thermal mismatch stresses and stresses resulting from dislocation pile-ups at grain boundaries. The residual thermal mismatch stresses provide the grain size dependence, while the dislocation pile-ups provide the time dependent aspect. A reduction in grain size leads to a reduction in thermal mismatch stresses, but also a reduction in slip length, thereby increasing the time to transition.

4. The active slip systems at the worn surface of alumina are quite different to that expected from bulk studies. While this maybe a strain rate effect, it is also believed to reflect the reduction of constraint at a surface and the possibly the effects of absorbed water.

5. So-called ceramic nanocomposites, based on Al_2O_3-SiC, do not appear to exhibit a time dependent wear transition. This is believed to be because of a change from intergranular to intragranular fracture. There is a greater propensity for dislocation activity at the worn surface of nanocomposites compared to monolithic alumina, but there is no evidence that this has the damaging consequences found in monolithic alumina associated with dislocation pile-ups at grain boundaries. While the nanocomposites exhibit mild wear over a much larger range of test conditions compared to monolithic alumina, wear rates in the mild wear regime may be greater for the nanocomposite.

6. The wear of zirconia ceramics is dominated by the low thermal conductivity of this material, which results in substantial flash temperatures, even under mild sliding conditions (e.g., 19 N load at 0.24 m/s can produce at least 800°C at the surface, probably much more). Since transformation of tetragonal to monoclinic zirconia is a low temperature mechanism, it is usually absent in the wear of these materials. The high temperatures promote severe surface deformation, including substantial grain shape change by dislocation flow, giving metal-like deformation structures. Water lubrication does not appreciably change this situation, with substantial temperature rises still detected, suggesting the water is excluded from the contacting interface. If the temperature is maintained low enough for transformation to occur, the associated microcracking can lead to enhanced wear rate where significant adhesive forces are present. As with alumina, substantial dislocation activity occurs below abrasive grooves, with transformation of the tetragonal zirconia to the monoclinic phase occurring some way below the surface.

Acknowledgements

The author is grateful to his co-collaborators who provided much of the original work presented here, including O. Barceinas-Sánchez, S. Bajwa, Y. Chen and R. Stevens. The author would also like to acknowledge the Engineering and Physical Sciences Research Council, who have provided funding over the years. Finally, the author is grateful to K. Adachi, K. Kato, B. Inkson, G. Mübus, H. Wu for the provision of original figures for inclusion here.

References

1. K. KATO and K. ADACHI, *Wear* **253** (2002) 1097.
2. K. ADACHI and K. KATO, *ibid.* **245** (2000) 84.
3. K. ADACHI, K. KATO and N. CHEN, *ibid.* **203–204** (1997) 291.
4. W. E. LEE and W. M. RAINFORTH, "Ceramic Microstructures" (Chapman & Hall, London, 1994).
5. S. W. LEE, S. M. HSU and M. C. SHEN, *J. Amer. Ceram. Soc.* **76** (1993) 1937.
6. M. C. SHEN and S. M. HSU, *Wear* **200** (1996) 154.
7. H. Y. LIU and S. M. HSU, *ibid.* **195** (1996) 169.
8. Y. WANG and S. M. HSU, *ibid.* **195** (1996) 35.
9. S. C. LIM and M. F. ASHBY, *Acta Metall.* **35** (1987) 1.
10. H. S. KONG and M. F. ASHBY, *MRS Bull.* **16** (1991) 41.
11. M. F. ASHBY, J. ABULAWI and H. S. KONG, *Tribol. Trans.* **34** (1991) 577.
12. P. ANDERSON and A. BLOMBERG, *Wear* **170** (1993) 191.
13. J. D. O. BARCEINAS-SANCHEZ and W. M. RAINFORTH, *Acta Mater.* **46** (1998) 6475.
14. S. J. CHO, B. J. HOCKEY, B. R. LAWN and S. J. BENNISON, *J. Amer. Ceram. Soc.* **72** (1989) 1249.
15. S. J. CHO, H. MOON, B. J. HOCKEY and S. M. HSU, *Acta Metall. Mater.* **40** (1992) 185.
16. B. J. HOCKEY, *J. Amer. Ceram. Soc.* **54** (1971) 223.

17. *Idem.*, *Proc. Br. Ceram. Soc.* **20** (1972) 95.
18. R. P. STEIJN, *J. App. Phys.* **32** (1961) 1951.
19. H. LIU and M. E. FINE, *J. Amer. Ceram. Soc.* **76** (1993) 2393.
20. K. P. D. LAGERLOF, T. E. MITCHEL, A. H. HEUER, J. P. RIVIERE, J. CADOZ, J. CASTAING and D. S. PHILLIPS, *Acta Metall.* **32** (1984) 97.
21. M. G. GEE, *Wear* **153** (1992) 201.
22. J. PEREZ-UNZUETA, J. H. BEYNON and M. G. GEE, *ibid.* **146** (1991) 179.
23. M. G. GEE, *J. Hard Mater.* **3** (1992) 363.
24. X. DONG, S. JAHANMIR and S. M. HSU, *J. Amer. Ceram. Soc.* **74** (1991) 1036.
25. A. NEVELOS, P. A. EVANS, P. HARRISON and W. M. RAINFORTH, *Proc. Inst. Mech. Engineers*, Part H. *J. Eng. Med.* **207** (1993) 155.
26. Y. S. WANG and S. M. HSU, *Wear* **195** (1996) 90.
27. C. HE, Y. S. WANG and S. M. HSU, *ibid.* **16**2 (1993) 314.
28. Y. S. WANG, C. HE, B. J. HOCKEY, P. I. LACEY and S. M. HSU, *ibid.* **181** (1995) 156.
29. S. JAHANMIR and X. DONG, *J. Tribology* **114** (1992) 403.
30. M. G. GEE, *Wear* **153** (1992) 201.
31. R. S. GATES and S. M. HSU, *Ceram. Trans.* **102** (1999) 67.
32. T. E. FISCHER, Z. ZHU, H. KIM and D. S. SHIN, *Wear* **245** (2000) 53.
33. R. C. WESTWOOD, N. H. MACMILLAN and R. S. KALYONCU, *J. Amer. Ceram. Soc.* **56** (1973) 258.
34. R. S. GATES, S. M. HSU and E. E. KLAUS, *Trib. Trans.* **32** (1989) 357.
35. J. T. CZERNUSZCA and T. F. PAGE, *Ceram. Surf. Surf. Treatm. Brit. Ceram. Proc. No. 3, Brit. Ceram. Soc.* (1984) 145.
36. *Idem.*, *J. Mater. Sci.* **22** (1987) 3917.
37. J. XU and K. KATO, *Wear* **245** (2000) 61.
38. A. RAVIKIRAN and S. JAHANMIR, *ibid.* **251** (2001) 980.
39. S. NOVAK, M. KALIN and T. KOSMAC, *ibid.* **250** (2001) 318.
40. K. NIIHARA and A. NAKAHIRA, in "Ceramics: Towards the 21st Century." The Ceram. Soc. of Japan. (1991) p. 404.
41. A. A. NAKAHIRA and K. NIIHARA, *J. Ceram. Soc. Jpn.* **100** (1992) 448.
42. K. NIIHARA, *J. Ceram. Soc. Jpn, Intern. Edit.* **99** (1991) 945.
43. C. C. ANYA, *Ceram. Intl.* **24** (1998) 533.
44. R. W. DAVIDGE and F. L. RILEY, *Wear* **186** (1995) 45.
45. R. W. DAVIDGE, P. C. TWIGG and F. L. RILEY, *J. Eur. Ceram. Soc.* **16** (1996) 799.
46. C. W. LAWRENCE, H. Z. WU, J. R. FRANCO, S. G. ROBERTS and B. DERBY, *Silicate Industr.* **63** (1998) 73.
47. H. KARA and S. G. ROBERTS, *J. Mater. Sci.* **37** (2002) 2421.
48. C. E. BORSA, S. JIAO, R. I. TODD and R. J. BROOKS, *J. Microsc.* **177** (1995) 305.
49. H. KARA and S. G. ROBERTS, *J. Amer. Ceram. Soc.* **83** (2000) 1219.
50. M. STERNITZKE, E. DUPAS, P. TWIGG and B. DERBY, *Acta Mater.* **45** (1997) 3963.
51. H. WU, B. J. INKSON and S. G. ROBERTS, *J. Microsc.* **201** (2001) 212.
52. H. WU, S. G. ROBERTS and B. DERBY, *Acta Mater.* **49** (2001) 507.
53. H. WU, C. W. LAWRENCE, S. G. ROBERTS and B. DERBY, *ibid.* **46** (1998) 3839.
54. H. Z. WU, S. G. ROBERTS, G. MÖBUS and B. J. INKSON, *ibid.* **51** (2003) 149.
55. J. RODRIGUEZ, A. MARTIN, J. Y. PASTOR, J. LLORCA, J. F. BARTOLOME and J. S. MOYA, *J. Amer. Ceram. Soc.* **82** (1999) 2252.
56. H. J. CHEN, W. M. RAINFORTH and W. E. LEE, *Scripta Mater.* **42** (2000) 555.
57. I. A. CHOU, H. M. CHAN and M. P. HARMER, *J. Amer. Ceram. Soc.* **79** (1996) 2403.
58. I. LEVIN, W. D. KAPLAN, D. G. BRANDON and T. WIEDER, *Acta Metall. Mater.* **42** (1994) 1147.
59. *Idem.*, *ibid.* **42** (1994) 1147.
60. J. X. FANG, M. P. HARMER and H. M. CHAN, *J. Mater. Sci.* **32** (1997) 3427.
61. S. BAJWA, PhD Thesis, The University of Sheffield, 2003.
62. W. M. RAINFORTH and R. STEVENS, *Wear* **162–164** (1993) 322.
63. B. J. INKSON, *Acta Mater.* **48** (2000) 1883.
64. M. WOYDT and K.-H. HABIG, *Ceram. Sci. Eng. Proc.* **9** (1988) 1419.
65. M. WOYDT, J. KADOORI, K.-H. HABIG and H. HAUSNER, *J. Europ. Ceram. Soc.* **7** (1991) 135.
66. W. M. RAINFORTH and R. STEVENS, *J. Mater. Res.* **13** (1998) 396.
67. W. M. RAINFORTH, *Ceram. Int.* **22** (1996) 365.
68. H. G. SCOTT, in Proc. Int. Conf. on Wear of Materials, edited by K. C. Ludema, Vancouver, Canada, 1985 (Am. Soc. of Mech. Eng., New York, 1985) p. 8.
69. L. J. LINDBERG and D. W. RICHERSON, in Proc. 2nd Int. Conf. on Ceram. Mater. and Components for Engines (Lubeck-Travemunde, 1986) p. 20.
70. C. S. YUST and F. J. CARIGNAN, *Wear* **28** (1984) 245.
71. S. T. GULATI, J. N. HANSSON, J. D. HELFINSTINE and C. J. MALARKEY, *Tube Intern.*, March (1985) 44.
72. R. H. J. HANNINK, M. J. MURRAY and M. MARMACH, in Proc. Int. Conf. on Wear of Materials, Reston, VA April, 1983, edited by K. C. Ludema (Am. Soc. of Mech. Eng., New York, 1983) p. 181.
73. R. H. J. HANNINK, M. J. MURRAY and H. G. SCOTT, *Wear* **100** (1984) 355.
74. J. BREZNAK, E. BREVAL and N. H. MACMILLAN, *J. Mater. Sci.* **20** (1985) 4657.
75. E. BREVAL, J. BREZNAK and N. H. MACMILLAN, *ibid.* **21** (1986) 931.
76. I. BIRKBY, P. HARRISON and R. STEVENS, *J. Europ. Ceram. Soc.* **5** (1989) 37.
77. A. TUCCI and L. ESPOSITO, *Wear* **172** (1994) 111.
78. M. V. SWAIN and R. H. J. HANNINK, *J. Amer. Ceram. Soc.* **72** (1989) 1358.
79. W. M. RAINFORTH, R. STEVENS and J. NUTTING, in Proc. lst European Ceramics Conference, edited by G. de With, R. A. Terpstra and R. Metselaar (Maastricht, Elsevier, 1989) Vol. III, p. 533.
80. W. M. RAINFORTH and R. STEVENS, in "Ceramic Transactions Vol. 17: Fractography of Ceramics II," edited by V. D. Frechette and J. R. Varner, Amer. Ceram. Soc. (1990) p. 363.
81. M. WOYDT, J. KLAFFKE, K.-H. HABIG and H. CZICHOS, *Wear* **136** (1990) 373.
82. T. E. FISCHER, M. P. ANDERSON, S. JAHANMIR and R. SALHER, *ibid.* **124** (1988) 133.
83. J. D. O. BARCEINAS-SANCHEZ and W. M. RAINFORTH, *J. Amer. Ceram. Soc.* **46** (1998) 6475.
84. G. W. STACHOWIAK and G. B. STACHOWIAK, *Wear* **132** (1989) 151.
85. *Idem.*, *ibid.* **160** (1993) 153.
86. *Idem.*, *ibid.* **143** (1991) 277.
87. R. RATNARAJAN, S. LAWSON and C. GILL, *Key Eng. Mat.* **99/100** (1995) 291.
88. Y. S. WANG and C. A. LEACH, *J. Mater. Sci.* **27** (1992) 5441.
89. S. LAWSON, *J. Europ. Ceram. Soc.* **15** (1995) 485.
90. W. M. RAINFORTH, *Wear* **245** (2000) 162.

Received 17 October 2003
and accepted 20 January 2004